LANGMUIR

pubs.acs.org/Langmuir Article

Dielectrophoretic Colloidal Levitation by Electrode Polarization in Oscillating Electric Fields

Xiaowen Chen, Xi Chen, Yixin Peng, Lailai Zhu, and Wei Wang*

Cite This: https://doi.org/10.1021/acs.langmuir.3c00759 Read Online

ACCESS | Metrics & More | Article Recommendations | Supporting Information

ABSTRACT: Controlled colloidal levitation is key to many applications. Recently, it was discovered that polymer microspheres were levitated to a few micrometers in aqueous solutions in alternating current (AC) electric fields. A few mechanisms have been proposed to explain this AC levitation such as electrohydrodynamic flows, asymmetric rectified electric fields, and aperiodic electrodiffusiophoresis. Here, we propose an alternative mechanism based on dielectrophoresis in a spatially inhomogeneous electric field gradient extending from the electrode surface micrometers into the bulk. This field gradient is derived from electrode polarization, where counterions accumulate near electrode surfaces. A dielectric microparticle is then levitated from the electrode surface to a height where the dielectrophoretic lift balances gravity. The dielectrophoretic levitation mechanism is supported by two numerical models. One model assumes point dipoles and solves for the Poisson−Nernst−Planck equations, while the second model incorporates a dielectric sphere of a realistic size and permittivity and uses the Maxwell-stress tensor formulation to solve for the electrical body force. In addition to proposing a plausible levitation mechanism, we further demonstrate that AC colloidal levitation can be used to move synthetic microswimmers to controlled heights. This study sheds light on understanding the dynamics of colloidal particles near an electrode and paves the way to using AC levitation to manipulate colloidal particles, active or passive.

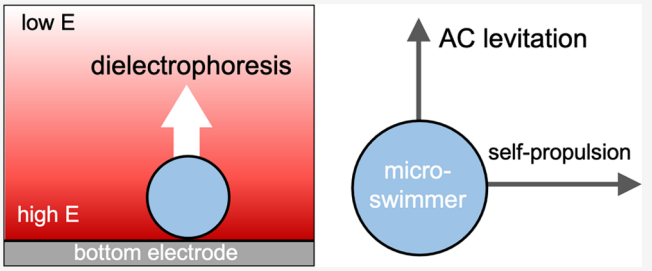

INTRODUCTION

The controlled transport of colloidal particles in all three dimensions holds significant values in a wide range of applications, ranging from bioanalysis and microassembly to particle sorting.[1−3] One bottleneck is the difficulty of levitating large quantities of colloids to controlled heights against gravity. Existing technologies are often limited in one way or another. For example, magnetic transport requires magnetic particles,[4−6] while levitating large numbers of particles to arbitrary heights with acoustic[7,8] or optical tweezers[9,10] is technologically challenging. Transporting colloids with an electric field, on the other hand, is appealing because its theory is well developed, it can be easily tuned, and it can be integrated with existing technologies such as microfluidics and structured light.[11] In particular, colloidal transport by alternating current (AC) electric fields has enjoyed wide success.[11,12]

Recently, it was reported[13,14] that 2 μm polystyrene (PS) microspheres suspended in HCl or NaOH aqueous solutions levitated from the surface of an electrode in an AC electric field oscillating at 100 Hz and of 40 V/cm. Later, similar colloidal levitation was achieved in NaSCN aqueous solutions under 1 kHz AC electric fields.[15] These observations suggest that AC levitation could be developed into a generic tool for manipulating colloids in 3D. Such AC levitation of colloidal particles was surprising, and a number of mechanisms were proposed to explain it including electrohydrodynamic (EHD) flows,[13] asymmetric rectified electric fields (AREFs),[16] and aperiodic electrodiffusiophoresis (EDP)[15] (see Results and Discussion for details). On the other hand, there is little information on the practical usefulness and limitations of using AC levitation as a technique to manipulate colloidal matter.

This study reports on the levitation of inert microspheres and synthetic microswimmers in AC electric fields of 10^2−10^4 Hz and in a few types of electrolytes. The key findings are twofold. First, we propose that AC levitation can be explained by dielectrophoresis (DEP)[17−19] of colloidal particles in a nonuniform electric field, which arises from the electrode polarization by counterions. Two numerical models of DEP were built, one assuming point dipoles and solving for 1D Poisson−Nernst−Planck equations, and the other a 3D finite-element multiphysics model that contained moving, polarizable spheres. Both models support (but do not conclusively confirm) dielectrophoretic levitation. Second, AC levitation is used to manipulate colloidal particles in 3D. Examples include

Received: March 21, 2023
Revised: April 26, 2023

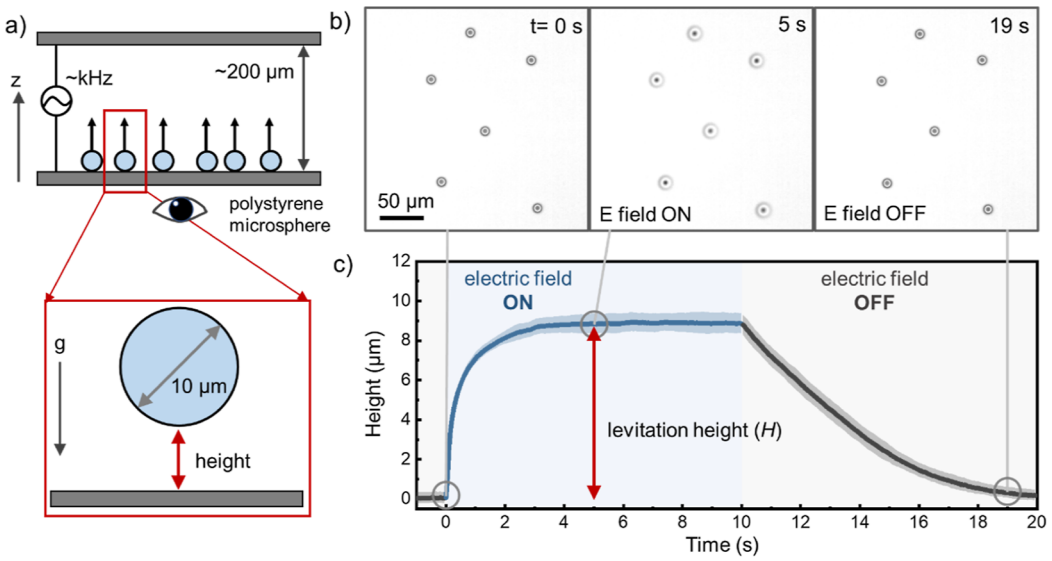

Figure 1. Levitation of colloidal particles in alternating electric fields. (a) Schematic of the experimental setup (not drawn to scale). Inset: a 10 μm microsphere levitated above an electrode. (b,c) Optical micrographs (b) and average heights of a population of PS microspheres (diameter = 10 μm) during levitation (0−10 s) and sedimentation (10−20 s) (c). Error bars in (c) represent standard deviations from 25 spheres. All experiments were performed in c_0 = 100 μM KCl aqueous solutions in an electric field of E_0 = 500 V/cm oscillating at f = 1 kHz. "Levitation heights" throughout this article are measured at t = 5 s, which is typically long enough for particles to reach their steady-state positions.

the sedimentation of colloidal populations from controlled heights and synthetic microswimmers controlled to move at variable heights. The potential contributions of other levitation mechanisms (most notably AREF and EDP) and the practical usefulness of AC levitation are also discussed.

AC levitation can potentially be developed into a versatile tool for sorting, assembling, and controlling colloids in 3D. On a more fundamental level, our findings provide refreshed insights into understanding the dynamics of colloidal particles near an electrode.

MATERIALS AND METHODS

Experimental Details. PS microspheres of various sizes and surface functionalities were purchased from vendors, and their product details and zeta potential are given in Tables S1 and S2 in the Supporting Information. The Janus microspheres shown in Figure 8a were fabricated by coating half of a 10 μm PS microsphere with ~1 nm of Pt with a low-vacuum sputter-coater (model SBC-12, KYKY). The experimental chamber for AC experiments was constructed by stacking together two pieces of coverslips coated with 200 ± 50 nm indium tin oxide (ITO, custom-ordered, 7−10 Ω/cm^2), with the ITO sides facing each other. A silicone spacer ~200 μm thick (custom-ordered, Gracebio) was placed in between. A wave function generator (model 33210A, Keysight) was connected to both ITO slides with copper tapes, and sinusoidal waves of typically 10 V (peak to peak) and 1 kHz were applied throughout this study. An inverted microscope (IX73, Olympus) was used to observe samples from below, and a CMOS camera (GS3-U3-41C6C-6, FLIR) was used to record movies and images, typically at 15 frames per second.

Particle Tracking. The 3D trajectories, and in particular the heights along z, of colloidal particles were obtained by a defocused-based algorithm (DefocusTracker) developed in ref 20, based on the principle that a colloidal particle defocuses differently at different heights for a fixed focal plane. In practice, a stack of images of different degrees of defocusing were acquired for a reference colloidal particle at different heights. This was done by manually turning the focusing knob on the microscope so that the focal plane of the objective lens was moved vertically without moving the sample stage. The algorithm then correlated each image with a specific height. Then, images taken from an actual experiment were compared to this reference stack to determine the particle's height. A schematic of this process and a stack of reference micrographs are given in Figure S1 in the Supporting Information. The particle coordinates on the xy plane were acquired by an in-house MATLAB code (courtesy of Prof. Hepeng Zhang from Shanghai Jiaotong University). Drift was minimal and thus not corrected by our tracking program in any of the three directions. The accuracy of this defocus-based tracking method is confirmed in Figure S2 by comparing it with results obtained by confocal laser scanning microscopy.

Calculation. Finite-element simulation software (COMSOL Multiphysics 5.4) was used to solve the point dipole and the moving, polarizable particle (MPP) models. In the point-dipole model, Poisson−Nernst−Plank equations were solved in 1D along the z direction. The MPP model was solved by COMSOL in a 2D axisymmetric configuration. It essentially solved for the same PNP equations as the point-dipole model but with a sphere of finite sizes in the box. In the MPP model, the electrical body force exerted on the particle was obtained by integrating the Maxwell-stress tensor over its surface, unlike the way DEP was calculated in the point-dipole model. The detailed implementation, including model geometries (Figure S3), parameter selection (Tables S3 and S4), and governing equations, of both models are given in the Supporting Information.

The electrical polarizability, i.e., Re(K), of a colloidal particle is calculated via eqs S22−29. The choice of parameters used in this equation is explained in Table S5. Only the leading order is used in eq 3 for calculating $\boldsymbol{F}_{\mathrm{DEP}}$, but higher-order multipolar moments are needed to calculate $\boldsymbol{F}_{\mathrm{DEP}}$ if the particle is placed in a strong field gradient. $\boldsymbol{F}_{\mathrm{DEP}}$ including the quadrupole moment is calculated by[21]

$$\boldsymbol{F}_{\mathrm{DEP}} = 2\pi\varepsilon_{\mathrm{m}}\nabla\left\{R^3\mathrm{Re}(K_1)[\boldsymbol{E}\cdot\boldsymbol{E}] + \frac{2}{3}\pi\varepsilon_{\mathrm{m}}R^5\mathrm{Re}(K_2)[\nabla\boldsymbol{E}\colon\nabla\boldsymbol{E}]\right\} \quad (1)$$

$$K_n = \frac{\varepsilon_{\mathrm{p}}^* - \varepsilon_{\mathrm{m}}^*}{n\varepsilon_{\mathrm{p}}^* + (n+1)\varepsilon_{\mathrm{m}}^*} \quad (2)$$

where the first and second terms in eq 1 correspond to the dipolar and quadrupolar terms, respectively. K_1 and K_2 are the Clausius−Mossotti factor calculated to the first and the second order, respectively. In Figure S4, we confirm that including higher-order terms significantly impacts the results only within ~2 μm near the electrode where the electric field gradient is large but does not

https://doi.org/10.1021/acs.langmuir.3c00759
Langmuir XXXX, XXX, XXX−XXX

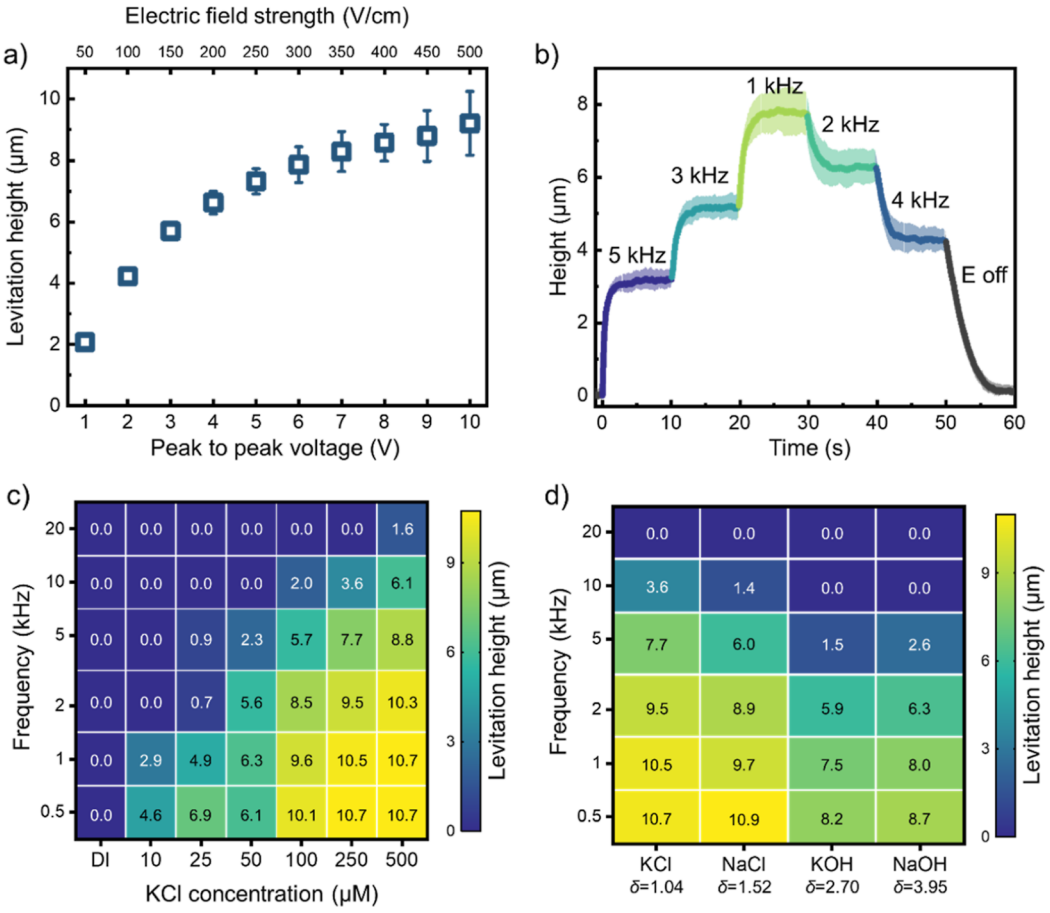

Figure 2. Levitation heights are varied with experimental parameters. Levitation heights at different driving voltages (a) and frequencies (b–d), as well as in electrolyte solutions of different concentrations (c) and types (d), for 10 μm PS microspheres. The levitation kinetics of (a) similar to that shown in Figure 1c are given in Figure S23. (b) A population of 10 μm PS microspheres is levitated to a sequence of controlled heights by varying the driving frequencies (E_0 = 500 V/cm; c_{KCl} = 100 μM). The levitation heights are color-coded in (c,d) so that smaller heights are blue and larger heights are yellow. Error bars in (a,b) represent standard deviations from approximately 30 and 15 spheres, respectively. Experiments in (a) were performed at 1 kHz and 100 μM KCl. Experiments in (c,d) were performed at 500 V/cm. Experiments in (d) were in 250 μM labeled electrolytes. $\delta = D_-/D_+$, where D_- and D_+ are the anion and cation diffusivity, respectively.

qualitatively change the calculated levitation heights. Higher-order corrections to $\boldsymbol{F}_{DEP}$ are therefore ignored for the rest of the study.

RESULTS AND DISCUSSION

Characterizing AC Colloidal Levitation at Kilohertz. In a typical experiment, PS microspheres 10 μm in diameter and a population density of 1.8% (defined as 2D packing fraction) were suspended in c_0 = 100 μM KCl and pipetted into a circular chamber ~200 μm tall sandwiched between two pieces of ITO glass slides. See Figure 1a for an illustration of the experimental setup. Unless otherwise noted, experiments were performed in a dilute suspension of colloidal particles separated by at least a few diameters. Therefore, interparticle interactions are not considered throughout this study. AC electric fields (φ_0 = 10 V peak to peak, corresponding to E = ~500 V/cm, sinusoidal) were applied perpendicular to the ITO electrodes typically at a driving frequency f of ~kHz (but can be varied from 500 Hz to 20 kHz in this study). Upon the application of AC fields, PS spheres initially settled on the bottom electrode moved against gravity and out of focus (Figure 1b and Movie S1), stopping at a few micrometers above the electrode within a few seconds.

The levitated microspheres would sediment back to the substrate when the electric field was turned off (Figure 1c). This provides a unique opportunity to study the sedimentation of a layer of colloids from controlled heights. For example, Figure S5a shows that a group of levitated colloids were allowed to freely sediment from different heights, and Figure S5b suggests that they sedimented more slowly as they approached the bottom because of hydrodynamic hindrance, in excellent agreement with the hydrodynamic prediction (see the Supporting Information for equations).

The coordinates of these microspheres in 3D were identified with high spatial and temporal precision with a defocus-based algorithm[20] (see Materials and Methods and Figure S1 for more details). In addition to high spatial precision, the unique advantage of such an algorithm over confocal microscopy used in previous studies of colloidal levitation[22] is the capability to follow the levitation kinetics of multiple particles with high temporal resolution (limited by our CMOS, typically at 15–30 fps). An example of such kinetics is shown in Figure 1c.

Throughout this article, z denotes the position along the normal of the planar electrode (i.e., the z direction) such that the surface of the bottom and top electrode of our cell is located at z = 0 and 200 μm, respectively. The height of a microsphere, on the other hand, is defined as the distance between its bottom to the top surface of the bottom electrode (see Figure 1a, inset). In reality, this height is not exactly 0 for

https://doi.org/10.1021/acs.langmuir.3c00759
Langmuir XXXX, XXX, XXX−XXX

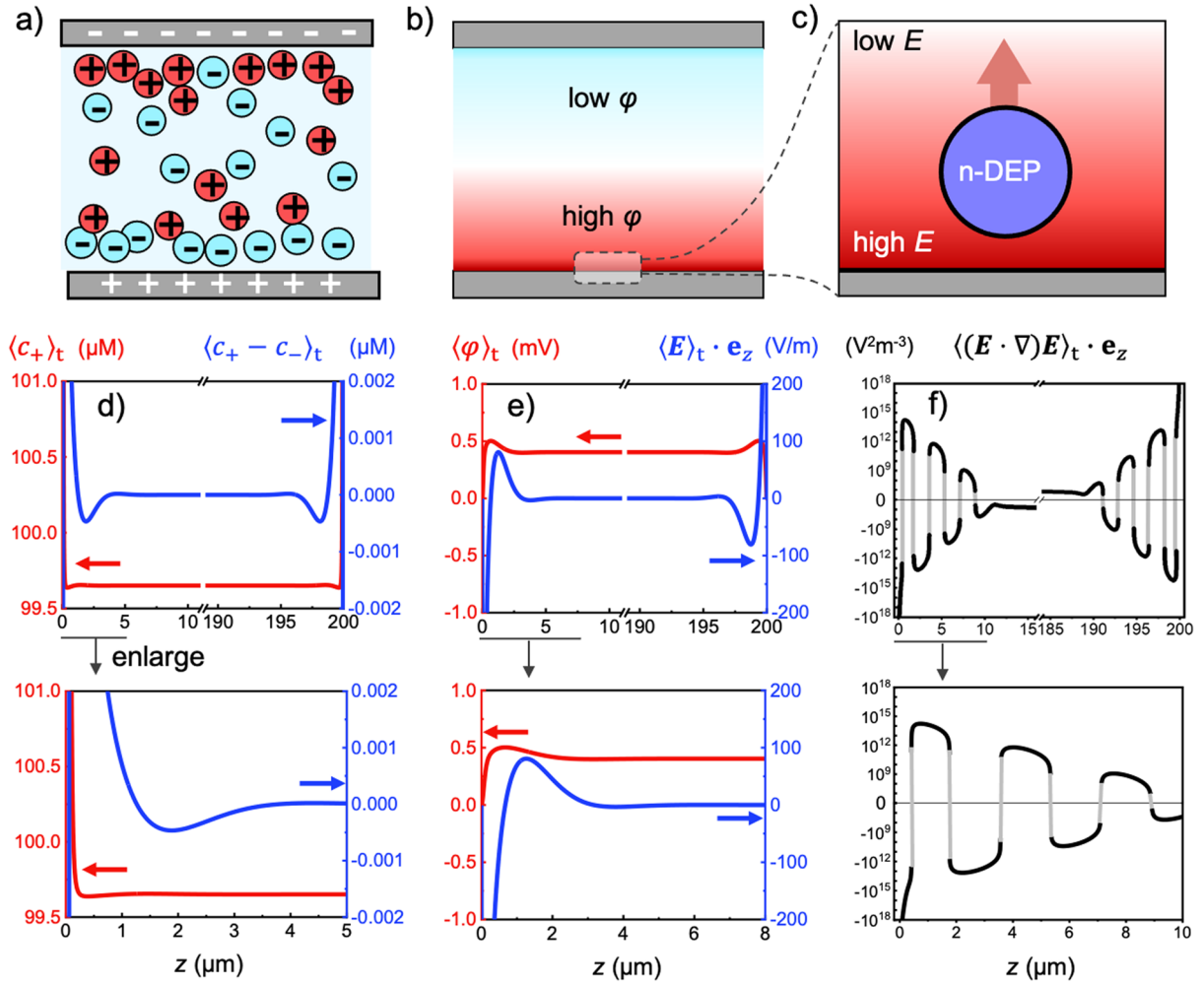

Figure 3. Dielectrophoretic levitation. (a−c) Over-simplified schematics of DEP near an electrode surface. Electrode polarization by counterions (a) leads to a distribution of electric potential across the bulk (b), which moves a dielectric microsphere that polarizes differently from the surrounding medium (negative DEP, or *n*-DEP, is given here as an example). (d−f) Time-averaged distributions of ions $\langle c \rangle_t$ (c_+ and c_- are the cation and anion concentration, respectively), electric potential $\langle \varphi \rangle_t$, the electric field strength $\langle \boldsymbol{E} \rangle_t$ and $\langle \boldsymbol{E} \cdot \nabla \boldsymbol{E} \rangle_t$ at E_0 = 500 V/cm, f = 1 kHz, and c_{KCl} = 100 μM ($\langle \rangle_t$ denotes time average). $\mathbf{e}_z$ is the unit vector along the z direction. These results were obtained by averaging the transient results within t = [5 s, 5.0001 s] (i.e., one oscillation cycle after 5 s) shown in Figure S6. The top row in (d−f) spans the entire 200 μm height (x-axes broken to highlight the changes near the electrodes), while the bottom row shows fine details near the bottom electrode (small z). The original results of (f) were not continuous near 0 along the vertical axis (see Figure S6d for example) after taking the logarithm. Gray lines were then hand-drawn to fill the gaps. The y axes in (d,e) are set to highlight the values a few micrometers away from either electrode. The actual maxima for $\langle c_+ - c_- \rangle_t$, $\langle \varphi \rangle_t$, and $\langle \boldsymbol{E} \rangle_t$ are ∼0.2 μM, ∼0.5 mV, and ∼3400 V/m, respectively (see Figure S26 for details).

a sedimented sphere because of the electrostatic repulsion between it and the substrate, as well as of Brownian motion. The finite thickness of this thin gap is taken into account in the simulation but ignored in the main text for conciseness. Finally, the levitation height H of a microsphere is defined as its height at the steady state (typically measured at t = 5 s after turning on an electric field).

The levitation heights of colloidal particles can be varied with experimental parameters. For example, PS microspheres levitated higher when higher electric field strength (Figure 2a) or lower driving frequencies (Figure 2b−d) were used, echoing previous studies on AC colloidal levitation.[13,22] Using this feature, Figure 2b and Movie S3 show how a layer of 10 μm PS spheres was levitated to different planes at different AC frequencies. In addition, particles levitated higher in more concentrated electrolyte solutions (Figure 2c), but the exact identity of the electrolyte is less critical because particles were levitated in KCl, NaCl, NaOH, or KOH aqueous solutions (Figure 2d). Particles generally levitated higher in KCl and NaCl than in KOH or NaOH. These results suggest that the levitation height of colloidal particles can be precisely tuned by careful choice of experimental parameters.

DEP: A Point-Dipole Model. We propose that the AC colloidal levitation described above and reported previously can be qualitatively explained by dielectrophoresis (DEP). DEP refers to the transport of objects in an electric field gradient, ∇E, and toward the point of the highest/lowest electric field strength for positive/negative DEP.[18,23] In our experiments, ∇E occurs because the applied electric potential at either electrode is quickly screened (over the order of the Debye length of $\approx O(10)$ nm in 100 μM KCl) by counterions migrating from the bulk toward the electrode surface. This process, known as electrode polarization[24−26] and shown schematically in Figure 3a, causes the electric potential to decay rapidly and nonlinearly from the electrode surface into the bulk. Intuitively, this results in a very large ∇E near the

https://doi.org/10.1021/acs.langmuir.3c00759
Langmuir XXXX, XXX, XXX−XXX

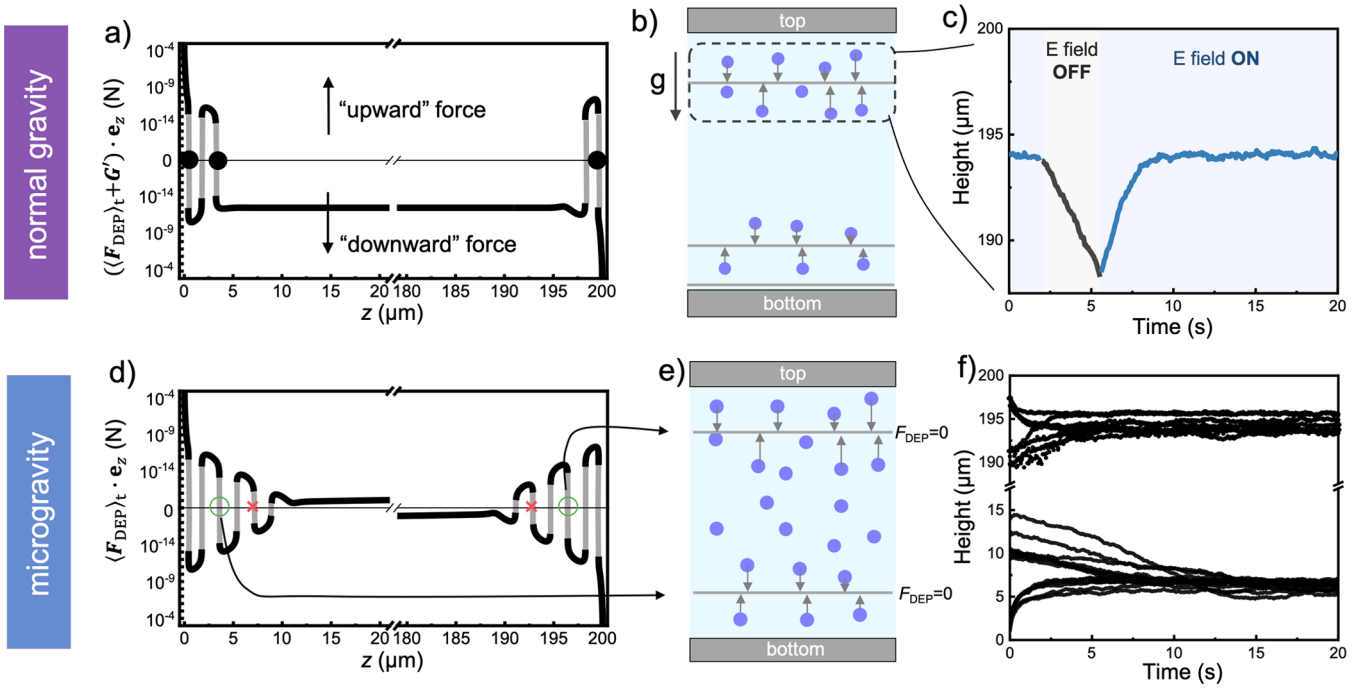

Figure 4. Dielectrophoretic trapping of colloidal particles to multiple heights under normal gravity (a–c) and in microgravity (d–f). (a,d) Time-averaged dielectrophoretic force $\langle \boldsymbol{F}_{DEP} \rangle_t$ calculated by the point-dipole method at different heights for 10 μm PS microspheres (E_0 = 500 V/cm, f = 1 kHz, Re(K) = −0.125, and c_{KCl} = 100 μM). Gaps in the calculated forces were connected manually with gray lines. The three black dots in (a) represent three stable levitation planes. Green circles in (d) correspond to the two levitation planes, while locations marked with red X indicate theoretical levitation planes that were not seen in experiments. The dielectrophoretic forces at these two points were likely too weak to overcome Brownian motion. (b,c) Schematic and tracking of the trapping of one 10 μm PS microsphere near the top electrode at E_0 = 500 V/cm, f = 3 kHz, and c_{KCl} = 100 μM. This microsphere was held ∼5 μm below the top electrode when the electric field was on but quickly settled by gravity when the field was turned off. Turning the electric field on again caused the particle to levitate back to the ∼5 μm spot. See Figure S25 and Movie S7 for the details of how this experiment was performed. (e,f) Schematic and tracking of 10 μm PS microspheres converging to two planes, one 6.3 ± 1.0 μm above the bottom electrode and the other 5.7 ± 1.1 μm below the top. The y axis in (f) is broken. Experiments in (f) were performed at E_0 = 500 V/cm, f = 5 kHz, and c_{KCl} = 100 μM. In (d–f), fluid was density-matched to PS ($\rho = 1.05 \times 10^3$ kg/m^3) by mixing water with D_2O ($\rho = 1.11 \times 10^3$ kg/m^3) at a volume ratio of 1:1.

electrode surface (Figure 3b). As a result, dielectric particles less polarizable than their surrounding medium move away from the electrode via negative DEP (Figure 3c) and thus levitation. Indeed, a previous study[27] showed that the calculated electric field strength near the electrode during electrode polarization was much larger than that in the bulk and used this effect to explain the preferential assembly of dielectric microspheres near an electrode. Note that "dielectrophoretic levitation" has been studied extensively, and electric field nonuniformities are typically created with interdigitated microelectrodes[28] or a curved electrode[29] to induce DEP of colloidal particles against gravity. In contrast, the DEP described in this study originates from field nonuniformities that evolve above and perpendicular to a planar, uniform electrode.

Dielectrophoretic levitation is a plausible mechanism because both DEP and electrode polarization are well-established effects. It is also well known that electrode polarization is stronger at low frequencies (<15 kHz) and low solution conductivities (<100 mS/m, corresponding to roughly 10 mM KCl[30]). These values are comparable with our experimental conditions. In fact, DEP is quite intuitive, so at one point, it was even considered for explaining AC levitation. However, this possibility was disregarded because the authors of ref 13 have estimated the magnitude of DEP and concluded that it is "...vanishingly small at the large micron-scale distances".[13]

On the contrary, we show below that DEP is not only non-negligible but can levitate colloidal particles micrometers into the bulk. The magnitude of the dielectrophoretic force $\boldsymbol{F}_{DEP}$ exerted on a microsphere is calculated by two methods. The first method, described in this section, assumes that the particle is small relative to the spatial inhomogeneities of the electric field so that it can be considered as a point dipole that polarizes without distorting the field around it. The time-averaged $\boldsymbol{F}_{DEP}$ (i.e., $\langle \boldsymbol{F}_{DEP} \rangle_t$, where $\langle \rangle_t$ denotes the time average) of this point-dipole model can then be calculated following (to the leading order)[17]

$$\langle \boldsymbol{F}_{DEP} \rangle_t = \langle (\boldsymbol{p} \cdot \nabla) \boldsymbol{E} \rangle_t = 4\pi \varepsilon_m R^3 \mathrm{Re}(K) \langle \boldsymbol{E} \cdot \nabla \boldsymbol{E} \rangle_t \quad (3)$$

where the polarizability $\boldsymbol{p}$ of a particle is related to the medium permittivity ε_m, the particle radius R, and Re(K), the real component of the Clausius–Mossotti factor K. Notably, $\boldsymbol{F}_{DEP}$ is a function of height because $\boldsymbol{E} \cdot \nabla \boldsymbol{E}$ changes along z, so the levitation height can be estimated by balancing $\langle \boldsymbol{F}_{DEP} \rangle_t$ with the buoyancy-corrected gravitational force. $\langle \boldsymbol{E} \cdot \nabla \boldsymbol{E} \rangle_t$ is solved by the one-dimensional Poisson–Nernst–Planck (PNP) equations[31] in the z direction

$$\text{Poisson's equation: } -\varepsilon_m \frac{\partial^2 \varphi}{\partial z^2} = \rho_e = Ze(c_+ - c_-) \quad (4)$$

https://doi.org/10.1021/acs.langmuir.3c00759
Langmuir XXXX, XXX, XXX–XXX

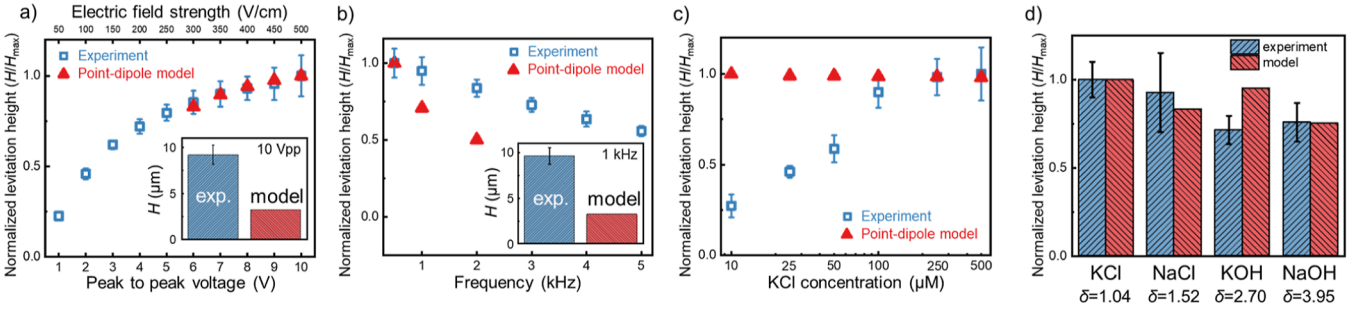

Figure 5. Levitation heights predicted by the point-dipole model and measured in experiments at different driving voltages (a), frequencies (b), electrolyte concentrations (c), or different types of electrolytes (d). Data in the main plots in (a) and (b) are normalized by their respective highest values, and one set of the actual values is given in each inset. Error bars represent standard deviations from approximately 30 spheres in (a,b) and approximately 25 spheres in (c,d). $\delta = D_-/D_+$, where D_- and D_+ are the anion and cation diffusivities, respectively.

$$\text{Nernst} - \text{Planck equation: } \frac{\partial c_\pm}{\partial t} = -\nabla \cdot J_\pm = \frac{\partial}{\partial z}\left(D_\pm \frac{\partial c_\pm}{\partial z} \pm Z\mu_\pm F c_\pm \frac{\partial \varphi}{\partial z}\right) \quad (5)$$

where ε_m is the permittivity of the medium, J is the ion flux, ρ_e is the space charge density, and c, μ, and D are the concentration, electric mobility, and diffusivity of the ions, respectively. The + and − signs correspond to the cation and anion, respectively. Z, e, and F are the ion valence, elementary charge, and the Faraday constant, respectively. Sinusoidal electric potentials $\varphi(t)$ were applied on the electrodes via $\varphi = \varphi_0 \sin(2\pi ft)$, where f is the driving frequency of the AC signal. The PNP equations were solved numerically using a finite-element solver COMSOL Multiphysics (see the Materials and Methods and Supporting Information). In particular, the transient results of c, φ, $\boldsymbol{E}$, and $\boldsymbol{E}\cdot\nabla\boldsymbol{E}$ along z at a pseudosteady state (see Figure S6) were averaged over one oscillation cycle to generate their respective time averages.

Figure 3d–f shows the establishment of temporally steady but spatially nonuniform (time-averaged) distributions of ions c, electric potential φ, and electric fields $\boldsymbol{E}$ between two electrodes of oscillating electric potentials. Importantly, $\langle \boldsymbol{E} \rangle_t$ is spatially nonuniform, so colloidal particles experience a dielectrophoretic force. The exact shapes and magnitudes of these distributions are sensitive to parameters such as the type of electrolytes (Figure S7a–d), the driving frequencies (Figure S7e–h), and voltages (Figure S7i–l) but are insensitive to the initial polarity of the electric field (i.e., which electrode was initially positive, Figure S8) or how the electrical potential was applied on either electrode as long as the electric potential difference between the two electrodes was the same (Figure S24).

The other key component in obtaining $\langle \boldsymbol{F}_{DEP} \rangle_t$ is the polarizability $\mathrm{Re}(K)$ of a colloidal particle of interest. The Supporting Information provides the equations for calculating $\mathrm{Re}(K)$,[32−34] and the result in Figure S9 indeed suggests that 10 μm PS spheres undergo negative DEP ($\mathrm{Re}(K) = -0.125$) in a typical experiment at 1 kHz and 100 μM KCl. Combining the above results of $\langle \boldsymbol{E}\cdot\nabla\boldsymbol{E} \rangle_t$ and $\mathrm{Re}(K)$ and following eq 3, Figure 4a shows the theoretical levitation heights at which the dielectrophoretic force is exactly balanced by the buoyancy-corrected gravitational force $\boldsymbol{G}'$ (i.e., $\langle \boldsymbol{F}_{total} \rangle_t = \langle \boldsymbol{F}_{DEP} \rangle_t + \boldsymbol{G}' = \boldsymbol{0}$). Three theoretical levitation heights are found for 10 μm PS spheres at z = 0.4, 3.2, and 199.6 μm. The one at z = 3.2 μm is close to the observed levitation height of 8.9 μm (Figure 4b), while the one very close to the bottom electrode at z = 0.4 μm is not observed. These two heights could explain the previous observation of the so-called "bifurcation",[13,14] where some particles levitate while others are trapped near the substrate. In addition, the model predicts a third levitation height very close to the top electrode. This was qualitatively confirmed by the observation of the trapping of 10 μm PS spheres 6 μm below the top electrode (Figure 4c). The presence of multiple levitation heights is better seen without the interference of gravity. For example, Figure 4d–f shows how 10 μm PS spheres initially suspended in a density-matched mixture of D_2O and H_2O rapidly formed two layers, each located a few micrometers away from one of the two electrodes. Moreover, Figure 4f shows that particles were trapped in experiments from both sides toward either levitation plane, consistent with the way dielectrophoretic forces are exerted. The locations of the two levitation planes were roughly symmetrical, both measured ~6 μm away from the electrode, in qualitative agreement with the prediction from the point-dipole model in Figure 4d.

Furthermore, the point-dipole model predicted that the levitation heights increase with increasing electric field strengths (Figure 5a) and decreasing driving frequencies (Figure 5b), in qualitative agreement with the experimental observations. However, the point-dipole model also makes a few predictions that are inconsistent with experiments. For example, the predicted levitation heights are consistently several times smaller than the experimental values. In addition, the point-dipole model predicts that levitation heights decrease slightly upon increasing ionic strengths (Figure 5c), while experiments showed the opposite trend. Moreover, Figure 5d shows inconsistency between experiments and model predictions for levitation heights in different electrolytes, especially in the case of NaCl and KOH. A potential source of these errors is the point-dipole assumption itself, which is unrealistic for 10 μm microspheres floating a few micrometers above an electrode. The absence of a physical sphere in the point-dipole model also introduces errors in the distribution of ions that cannot penetrate the particle, and/or in the distribution of the electric field that is distorted by the particle.

DEP: A Moving, Polarizable Particle Model. Given the fundamental limitations of the point-dipole method described above, a second model containing a moving, polarizable particle (called the MPP model) was constructed to calculate the dielectrophoretic forces on microspheres near an electrode. Same as the point-dipole model, the MPP model solved for the

https://doi.org/10.1021/acs.langmuir.3c00759
Langmuir XXXX, XXX, XXX−XXX

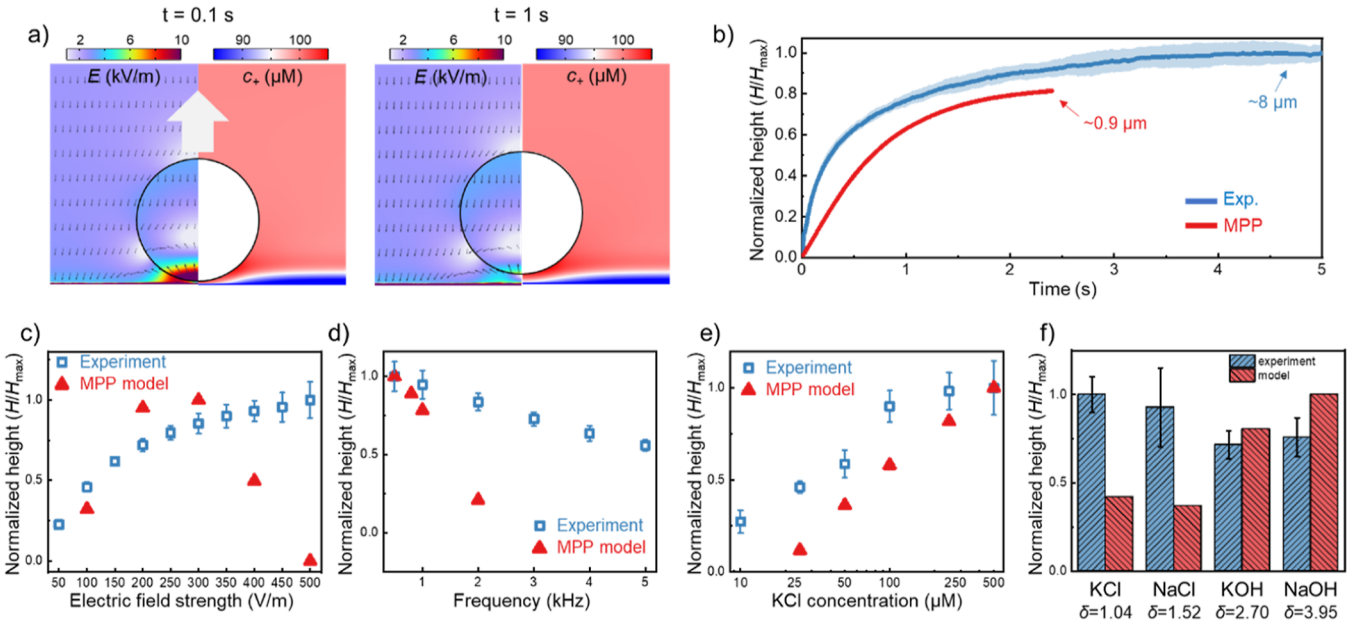

Figure 6. Levitation heights predicted by the MPP model for 10 μm PS spheres. (a) Distribution of the electric field $\boldsymbol{E}$ (the contour color and arrows indicate its norm and direction, respectively) and the cation concentrations c_+ at t = 0.1 s (left) and t = 1 s (right). The applied electric potential is exactly 0 in these two instances. Transient results from other time instances within one period are given in Figure S11. (b) Levitation kinetics from experiments and the MPP model in a cell 100 μm tall, at E_0 = 300 V/cm, c_{KCl} = 100 μM, and f = 1 kHz. The experimental data in (b) are normalized by the levitation heights at t = 5 s (~8 μm), while the simulated data in (b) are normalized by a steady-state levitation height of 1.1 μm. This value was not obtained by running the simulation for long enough, which was extremely costly in computational time, but by finding the height where the dielectrophoretic force on a particle is exactly balanced by its gravitational force (see Figure S12). (c–f) Comparison between experimental and simulated heights at different voltages, frequencies, c_{KCl}, and types of electrolytes, respectively. Experimental data were obtained at t = 5 s, while MPP simulation data were obtained at t = 0.5 s (thus, not the steady state) and normalized by their respective maxima. Experimental errors of the experimental data in (b–f) represent standard deviations from the measured heights of 20–60 microspheres. Parameters of experiments in (c–f): h = 200 μm, R = 5 μm, and φ_0 = 10 V_{pp} (d–f), f = 1 kHz (c,e,f), and c_0 = 100 μM (c,d,f). Parameters of the MPP model in (c–f): h = 100 μm, R = 5 μm, φ_0 = 3 V_{pp} (d,e,f), f = 1 kHz (c,e,f), and c_0 = 100 μM (c,d,f).

ion transport and electrostatics in an aqueous solution between two electrodes according to the PNP equations. However, three distinctive features of the MPP model are as follows: (1) it incorporated a dielectric sphere of a realistic size and permittivity so that it produced distributions of ions and electric potential near an electrode that were markedly different from those predicted by the point-dipole model; (2) the microsphere was allowed to move in the model while being solved so that levitation kinetics could be obtained; (3) $\boldsymbol{F}_{DEP}$ in the MPP model was not obtained from eq 3 as in the point-dipole method but was calculated by integrating a Maxwell-stress tensor over the particle surface (eqs S10 and S11), which is essentially the electrostatic body force on the particle exerted by the electric field [also known as the Maxwell-stress tensor formulation[35,36]]. A few assumptions were made to simplify the model: the particles carried no intrinsic surface charge (so the zeta potential was 0, and any kind of electrophoresis was ignored); there was no electrochemical reaction on the electrode surface; only ions from the chosen electrolyte (KCl, NaOH, etc.) were present (so protons and HCO_3^- from the dissolution of CO_2 in water were ignored); fluid flows were not considered (so convective transport of ions was ignored).

The MPP model was solved numerically by COMSOL Multiphysics with a moving mesh (see the Supporting Information for details). The electrical permittivity of the microsphere was set to be that of PS (ε_p = 2.55), which was smaller than that of water (ε_p = 78.5) so that it undergoes negative DEP as predicted by the Re(K) calculations in Figure S9. Note that MPP models are prohibitively expensive in terms of computational time, so transient simulations beyond a typical time duration of 1–2 s were not unfeasible. Steady-state levitation heights were therefore not obtained. The validity of the MPP model is supported by Figure S10, where the point dipole and the MPP model predicted similar steady-state levitation heights for a microsphere 1 μm in diameter (small enough for the point dipole assumption to be reasonable). This similarity suggests that the MPP model faithfully captures the key features of DEP.

Based on the principle of DEP, the MPP model produced nonlinear distributions of ions and electric potential near the bottom electrode and reproduced the levitation of a 10 μm PS microsphere (Figure 6a). Moreover, and without any fitting parameters, the MPP model predicted transient levitation kinetics that were qualitatively (but not quantitatively) consistent with the experimental measurements (Figure 6b). Quantitatively, the MPP model predicted higher levitation at higher voltages (Figure 6c), at lower driving frequencies (Figure 6d), and in more concentrated KCl solutions (Figure 6e), all of which were in qualitative agreement with the experiments. However, the MPP model predicted lower levitation heights in electrolytes of smaller δ (Figure 6e), contrary to the experiments. Notably, the transient particle heights calculated by the MPP model were consistently lower by a large margin than those measured experimentally after the same elapsed time. These inconsistencies between the MPP model and the experiments suggest that, although the MPP

https://doi.org/10.1021/acs.langmuir.3c00759
Langmuir XXXX, XXX, XXX–XXX

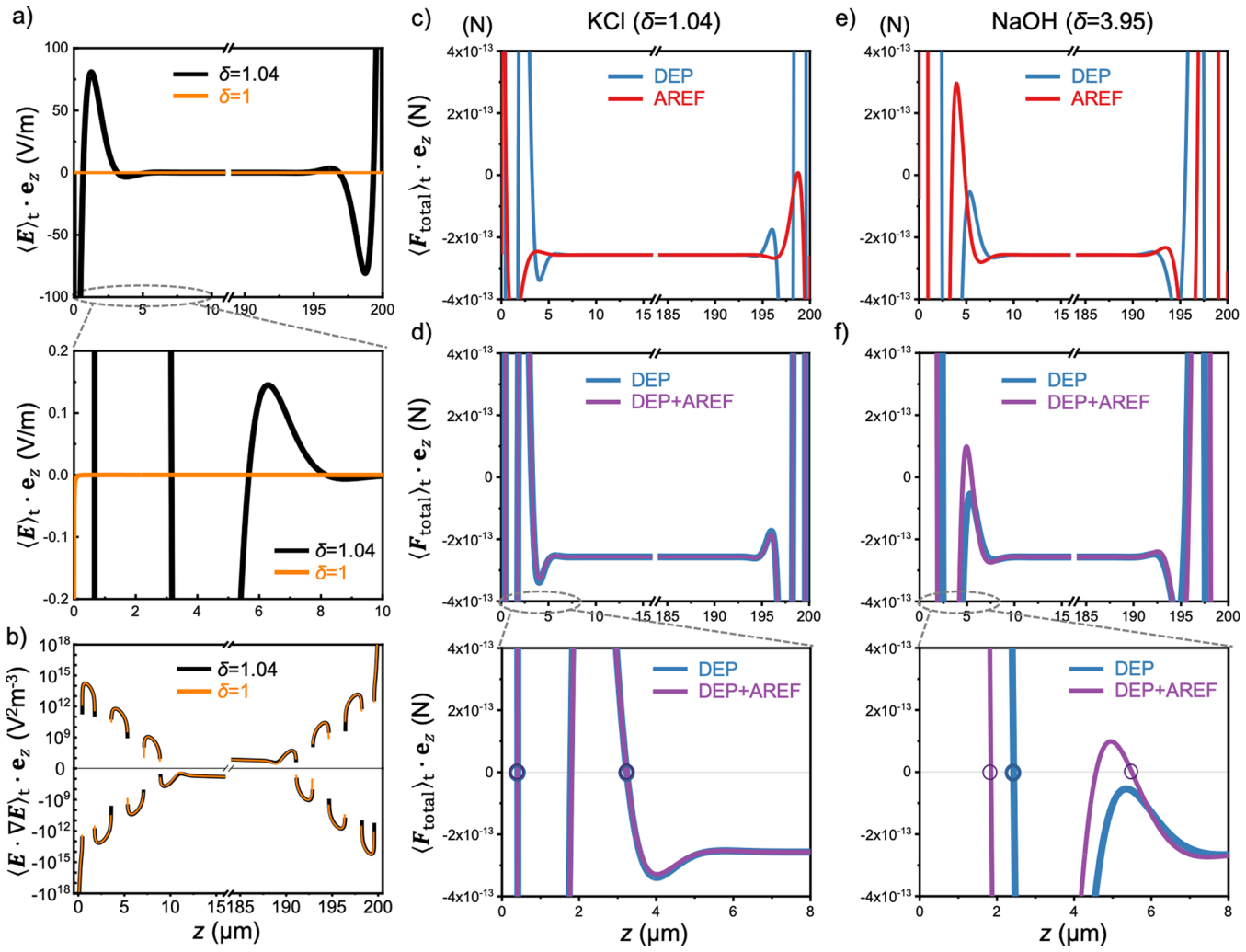

Figure 7. Comparing DEP to AREF. (a,b) Spatial distributions of $\langle \boldsymbol{E} \rangle_t$ and $\langle \boldsymbol{E} \cdot \nabla \boldsymbol{E} \rangle_t$ in 100 μM electrolytes of δ = 1 (orange line) and δ = 1.04 (black line, corresponding to KCl) in AC electric fields of f = 1 kHz and E_0 = 500 V/cm. Although the shapes of $\langle \boldsymbol{E} \rangle_t$ are quite different between results obtained with δ = 1 and 1.04, those of $\langle \boldsymbol{E} \cdot \nabla \boldsymbol{E} \rangle_t$ are similar for both cases, suggesting similar distributions of the dielectrophoretic forces for particles immersed in these two electrolytes. (c−f) Effect of including AREF in the levitation of 10 μm PS microspheres at E_0 = 500 V/cm, f = 1 kHz, and in 100 μM KCl (δ = 1.04, (c,d)) and NaOH [δ = 3.95, (e,f)]. The stable levitation heights in each case are labeled with circles. All distributions and forces in this figure are calculated by the point-dipole model.

model is a more powerful and realistic model than the point-dipole model, it is not perfect.

One source of such inconsistency could be that the MPP model made a few assumptions that ignored some potentially important components, as described above. As a first step toward a more complete model, we show in Figure S13 that a revised MPP model including hydrodynamics produced significantly larger transient levitation heights than a model without hydrodynamics. This result is promising, but an MPP model that includes all of the missing components mentioned above is unfortunately beyond our current capabilities.

Potential Levitation Mechanisms besides DEP. EHD flows were the first mechanism proposed to explain AC colloidal levitation (Figure S15a):[13] a colloidal particle sitting above an electrode distorts the vertical electric field so that the horizontal component of the distorted electric field couples to the charged electrode to generate a lateral electroosmotic flow, known as an EHD flow.[37] Under the appropriate experimental conditions, this flow converges on the particle and lifts it by fluid continuity, resulting in levitation. However, this EHD mechanism cannot fully explain AC levitation for four compelling reasons. First, the magnitude of EHD flows is known to scale with $1/z^3$,[13] where z is the height above the substrate so that the EHD flow would be extremely weak for a particle levitated ∼10 μm above the substrate as in Figures 1 and 2. Second, our experiments in Movie S2 suggest that EHD flows are neither sufficient nor necessary for levitation because particles were still able to levitate in weak EHD flows but did not necessarily levitate in strong EHD flows. Third, Figure S16 suggests that the strength of EHD flows is inversely proportional to the ionic strength. However, results in Figure 2b clearly indicate higher levitation in more concentrated salt solutions, contrary to what EHD predicts. Finally, Figure 4 shows that colloidal particles can be trapped near both the bottom and the top electrodes in an AC electric field, but EHD cannot both push and pull under the same experimental condition.

An alternative mechanism is the recently proposed aperiodic EDP.[16] The key idea is that electrochemical reactions occurring at the electrode surface generate long-range pH gradients, as convincingly demonstrated by the author of ref 15. As a result, electrically charged colloidal particles move via

https://doi.org/10.1021/acs.langmuir.3c00759
Langmuir XXXX, XXX, XXX−XXX

electrolyte diffusiophoresis to the point of highest pH, where they are trapped. It is reasonable to suspect that EDP plays a role in our experiments because electrochemical reactions are possible in our experiments at driving frequencies of kilohertz and below. These frequencies are only a few times larger than the critical frequency for Faradaic processes to occur (calculated according to ref 38 to be a few hundred Hertz in 100 μM KCl). Moreover, water electrolysis has been reported under experimental conditions similar to those used here even though bubbles were not observed.[15] Confirmation of the possible contribution of EDP in our experiments requires careful measurement of pH gradients, accurate modeling of the electrochemical reactions at the electrodes, and possibly blocking the electrode surface to minimize electrochemical reactions. Unfortunately, none of these are within our current capabilities.

The last, but not least, mechanism is based on the so-called AREF (Figure S15b). In brief, the AREF mechanism states that electrode polarization in an AC electric field leads to a time-averaged, steady electric field ($\langle \boldsymbol{E} \rangle_t$).[16,22,39−41] An electrically charged colloidal particle therefore levitates by electrophoresis to a height where the electrophoretic lift balances gravity. The AREF mechanism has two key requirements: an electrolyte of $\delta \neq 1$ and particles that carry substantial surface charges.

The point-dipole model of our DEP mechanism is both similar to and different from the AREF mechanism. They are similar because both arise from the same electrode polarization process, both are based on the same PNP equations of eqs 4 and 5, both assume point dipoles, and both produce the same inhomogeneous distributions of c, φ, and $\boldsymbol{E}$ (such as that shown in Figure 3). However, the AREF model solved for $\boldsymbol{E}$, leading to electrophoresis via $\boldsymbol{F}_{EP} = 6\pi R\varepsilon_m\zeta_p\boldsymbol{E}$, while we instead solved for $\boldsymbol{E}\cdot\nabla\boldsymbol{E}$, leading to DEP via eq 3. Thus, the two mechanisms differ fundamentally in what is ultimately responsible for levitation—DEP or electrophoresis. This difference is perhaps most striking for the electrolyte of $\delta = 1$ (Figure 7a,b), in which case AREF vanishes because $\langle \boldsymbol{E} \rangle_t$ is negligible except for being very close to the electrode surface so that bulk electrophoresis disappears. However, DEP would still operate when $\delta = 1$ because $\langle \boldsymbol{E}\cdot\nabla\boldsymbol{E} \rangle_t$ is large enough to generate substantial dielectrophoretic forces even a few micrometers away from the electrode.

Despite this difference, the effect of AREF must be present in our experiments because $\delta \neq 1$ for all electrolytes used in our experiments. The results in Figure 7c−f quantify the contribution of AREF and suggest that AREF is negligible in our experiments with KCl ($\delta = 1.04$, Figure 7c,d) but potentially significant in experiments with NaOH ($\delta = 3.95$, Figure 7e,f). However, the same results also suggest that, under the combined effect of DEP and AREF, particles would levitate higher in NaOH than in KCl (5.5 vs 3.2 μm), contrary to our experimental measurements in Figure 2, which shows higher levitation in KCl than in NaOH. We cannot yet explain this discrepancy, but it could be due to the point-dipole approximation used in both mechanisms, which as we explained earlier is inaccurate for 10 μm microspheres close to an electrode. Note that the MPP model we used to calculate DEP excludes the contributions of AREF because particles are not charged in this model, and any levitation it predicts is thus solely due to DEP.

DEP from electrode polarization is a strong candidate to explain AC colloidal levitation. Not only is it based on well-established theories of DEP and on the well-recognized effect of electrode polarization, but it is also applicable to a wide range of experimental conditions including in electrolytes of $\delta = 1$ (Figure 7a,b), or with particles having little or no surface charge, or under high driving frequencies or low voltages unable to cause electrochemical reactions on the electrodes. AREF or EDP does not work well under these conditions. Similar to AREF and EDP, particles of a wide variety of materials can in principle be levitated by DEP; although this study has focused on negative DEP, Figure S17 predicts that positive DEP can also levitate particles by a few micrometers near both electrodes.

However, we do acknowledge that the DEP mechanism proposed here is limited. Notably, the point-dipole model is physically unrealistic for large spheres near an electrode. Perhaps because of this, this model under-calculates the levitation heights and predicts that these heights change with electrolyte types and concentrations in a way that is inconsistent with experiments (see Figure 4). The MPP model, while more realistic, is extremely slow to solve and also predicts levitation heights that are much smaller than experimental values (see Figure 6).

Given these limitations, a potential method to qualitatively validate DEP and identify the contributions of AREF and EDP is to experiment with either (1) particles of $\mathrm{Re}(K)$ of exactly 0, so that DEP disappears, or (2) particles of negligible surface charge to remove EDP or AREF since both are based on electrophoresis and thus require surface charges. However, these experiments are technically challenging. As a compromise, we tested two types of 5 μm PS microspheres, one fluorescently labeled and the other not, both carrying similar amounts of surface charges. Figure S18 shows that the fluorescent microspheres were unable to levitate in 100 μM KCl and a 1 kHz AC field, while the nonfluorescent microspheres levitated to 6 μm. DEP experiments with interdigitated microelectrodes (Figure S19) suggested that the two types of PS microspheres had opposite polarizability, which is suspected to be due to the difference in their surface coating or the way the dyes were incorporated (such information is propriety and not available at this moment). Their difference in levitation can only be tentatively explained by DEP but not by AREF or EDP and serves as preliminary evidence of the dielectrophoretic levitation mechanism.

Although the evidence reported in this article suggests that DEP is a plausible mechanism to explain AC colloidal levitation, the alternative mechanisms discussed above—EHD, AREF, and EDP—could dominate at different frequencies, at different particle−wall distances, or for particles with different physicochemical properties. For example, AREF could become more important or even dominant for small particles (because $\boldsymbol{F}_{DEP}$ scales with R^3) or for electrolytes of high δ, whereas DEP could dominate in the cases of large particles or δ close to 1. EDP, on the other hand, could dominate for large applied voltages and/or small driving frequencies that produce large ion fluxes on the electrode surfaces. Both AREF and EDP become more important for particles with larger surface charges. Finally, EHD is typically strong at low driving frequencies below 1 kHz. It is also possible that many or all of the above mechanisms may occur simultaneously and thus contribute collectively to AC levitation. Elucidating their exact contributions, and confirming the presence and magnitude of DEP, would require substantial effort and is beyond the scope of this study.

https://doi.org/10.1021/acs.langmuir.3c00759
Langmuir XXXX, XXX, XXX−XXX

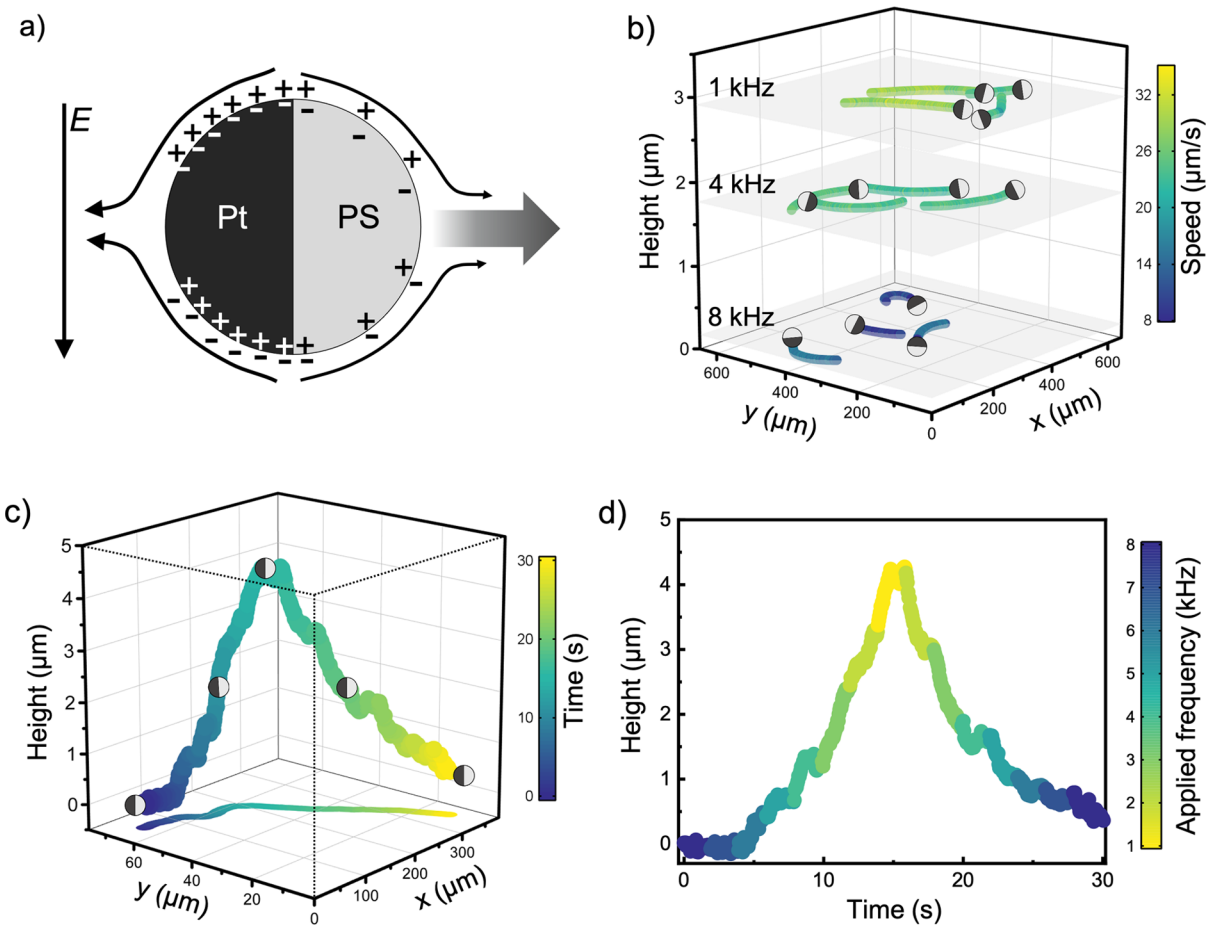

Figure 8. Manipulating synthetic microswimmers in 3D with AC levitation. (a) Propulsion of a metal-dielectric Janus microsphere in an AC electric field. The two hemispheres polarize differently, producing a steady-state osmotic flow that moves the particle away from its metal side via ICEP. (b) PS microspheres 10 μm in diameter half-coated with ~1 nm of Pt moving autonomously via ICEP at three different heights. They were levitated by AC electric fields of 8, 4, and 1 kHz, respectively (E_0 = 250 V/cm, in 100 μM KCl). On each plane, the 10 s trajectories of a few representative swimmers are indicated with their color-coded instantaneous speeds. The heights of the two levitation planes were the average of the z coordinates of all tracked swimmers (n = 4) on that plane. (c) 3D trajectory of a representative Pt-PS swimmer and its 2D projection on the xy plane during the continuous tuning of the driving frequencies (E_0 = 200 V/cm, in 100 μM KCl). Both trajectories are color-coded with time. (d) Heights of the swimmer in (c) over time, color-coded with the instantaneous driving frequencies.

Using AC Levitation to Move Synthetic Microswimmers in 3D. Controlled levitation of colloidal particles by AC electric fields enables the 3D manipulation of large populations of colloidal particles. For example, the levitation height of a population of PS microspheres can be precisely controlled by varying the driving voltage or frequency because of their direct effect on $\boldsymbol{F}_{\mathrm{DEP}}$ (i.e., Figure 2). Using the same principle, AC levitation can also be applied to raise or lower colloidal particles that autonomously move, also known as synthetic microswimmers, active colloids, micromotors, or colloidal motors.[42,43] Synthetic microswimmers that swim in 3D could benefit applications such as biosensing[44] or environmental remediation,[45] and they are also a useful model system for understanding active matter.[46,47] In addition, levitating synthetic microswimmers enables the study of their propulsion far from any boundary,[48] which is known to affect not only their speeds[49−55] but also their orientations[56−59] and collective behaviors.[60] In reality, however, a synthetic microswimmer typically moves in 2D because they are often heavier than water and tend to accumulate near boundaries.[61,62] To force them to move away from an interface often requires tilting their engines downward by gravity[63−65] or external torques[66] or by acoustically levitating them to the bulk.[67] Both strategies compromise the swimmer's ability to swim freely.

AC levitation offers a new strategy for propelling synthetic microswimmers in free space. For example, Figure 7a,b shows 10 μm PS microspheres with a very thin Pt cap (see Materials and Methods for details) that were levitated to different heights by AC electric fields. They underwent negative DEP despite a thin metal coating, which was confirmed by experiments with interdigitated microelectrodes (Figure S14). In addition to levitation, these metal-dielectric Janus microspheres are also self-propelled in AC electric fields via the so-called induced charge electrophoresis (ICEP,[68,69] Figure 8a). They then swam freely on these levitational planes of adjustable height. Figure 8c,d and Movie S5 further demonstrate how a single swimmer can continuously float or sink while maintaining horizontal propulsion. Importantly, the independent trajectories in Figure 8b and Movie S4 suggest that AC levitation imposes no directional constraints on these swimmers, thus allowing them to freely explore the entire levitational plane with reorientation solely caused by Brownian diffusion. To the best of our knowledge, this is the first experimental demonstration of synthetic microswimmers

https://doi.org/10.1021/acs.langmuir.3c00759
Langmuir XXXX, XXX, XXX−XXX

moving autonomously at controlled heights in free space. Combining our recent experiment of dielectrophoretically guiding the trajectories of synthetic microswimmers in 2D with the optoelectronic effect,[70] it is possible to envision precise control of microswimmers in 3D entirely by DEP.

Practical Considerations for Using AC Colloidal Levitation. In addition to the examples described above, the usefulness of AC levitation can be extended in several directions. First, AC levitation could be used to study how hydrodynamic interactions among colloids trigger interesting settling instabilities.[71] Compared to other techniques such as acoustic levitation,[72] AC levitation confers the unique advantage to move a colloidal population to controlled heights in a liquid without introducing additional effects. Second, a synthetic microswimmer levitated by DEP can be further coated with a magnetic layer (e.g., iron oxides or Ni) to enable its 3D steering along arbitrary, programable trajectories. This is useful for sensing,[44] cargo transport,[73,74] and decontamination[45] with microrobots in the bulk. Finally, DEP and AC levitation could potentially explain the irreversible adhesion of colloidal particles (especially those containing metals) often observed in an AC electric field.

A few practical considerations for using AC levitation are:

- Size. Experimentally, we found that it was easy to levitate 10 and 5 μm PS microspheres a few micrometers above the bottom electrode, while 500 nm PS spheres were instead attracted to the electrode surface (see Movie S6). Although we could attempt to rationalize this observation using the point-dipole model, realistically, the physical presence of the particles makes the distributions of ions and electric potential less intuitive. This issue is further complicated by the fact that the polarizability of a colloidal particle is sensitive to its size. We therefore caution against prematurely predicting that a particular type of microsphere will or will not levitate.

- Density. AC levitation does not work well for heavy particles such as pure metal colloids, likely because metal particles are too heavy for the dielectrophoretic force to counteract (see Figure S20 for the $\langle \boldsymbol{F}_{\text{total}} \rangle_t$ profile of a gold microsphere). However, dielectric colloids coated with a very thin metal layer can still levitate (such as the PS-Pt spheres shown in Figure 8). On the other hand, typical dielectric colloidal particles such as polymers and silicon dioxide (SiO_2) of relatively large sizes levitate well (Figure S21), and levitation is in general easier with a stronger electric field, lower driving frequencies, and higher ionic strength (see Figure 2). Under optimal conditions, we have found that a 10 μm PS microsphere could levitate to a maximum of 10.7 μm at 500 V/cm, 500 Hz, and in 0.5 mM KCl. They could be levitated even higher if a density-matched medium was used.

- Interactions among levitated particles. As is typical for colloidal particles in an electric field,[27,75] those levitated by AC electric fields still experience electrical dipolar interactions that repel particles on the same horizontal plane but attract those that are vertically aligned. This becomes important for more concentrated suspensions, and we have indeed seen levitated microspheres form chains along the field line (Figure S22). The in-plane repulsive interaction, on the other hand, makes it theoretically possible to produce a levitated 2D colloidal crystal with tunable spacing. This possibility has yet to be tested.

CONCLUSIONS

This study reports the levitation of 10 μm PS microspheres up to 10.7 μm in AC electric fields of 50−500 V/cm, 500 Hz−20 kHz, in electrolytes such as KCl, NaCl, KOH, and NaOH of 10−500 μM. Experimentally, we found that particles levitated higher in stronger electric fields, at lower driving frequencies, and in more concentrated electrolyte solutions (up to 500 μM). Moreover, particles levitated higher in KCl and NaCl than in KOH or NaOH. A mechanism based on dielectrophoresis (DEP) was proposed to explain such levitation. DEP arises from electrode polarization by counterions, which generates nonuniform electric fields between the two electrodes. A dielectric particle then moves by DEP in $\nabla \boldsymbol{E}$ until the lift is balanced by gravity. Two models were built to calculate the dielectrophoretic forces, one assuming point dipoles and the other containing a moving, polarizable particle. Although both models could qualitatively reproduce AC levitation, neither model was in perfect agreement with the experiments, either in terms of the exact heights of levitation or the way in which the heights of levitation varied with some experimental parameters. It is possible that other mechanisms, such as EHD, AREF, or EDP, could contribute to AC levitation to varying degrees under different experimental conditions, and we are yet to reach a conclusion on which mechanism dominates. In addition, we have also used AC levitation for manipulating colloidal particles in 3D, particularly in the controlled floating and sinking of synthetic microswimmers. Several practical considerations when using AC levitation were discussed, such as particle sizes, density, and particle−particle interactions.

Our proposed mechanism based on DEP, despite being preliminary, provides an intuitive, self-consistent, and thus compelling framework for understanding the coupling between colloidal electrokinetics and electrode polarization. The key element in this mechanism is the steady-state, time-averaged distribution of ions, electric potentials, and electric fields that are highly nonuniform in space and that extend from the electrode surface ~10 μm into the bulk, even when the cation and the anion migrate at equal rates or when the particle carries no electric charge. Such a nonlinear effect could inspire new thinking about how colloids behave near interfaces beyond the levitation we focused on here. From an applied point of view, our results suggest that AC levitation could be developed into a versatile and precise method for controlling colloidal particles (and microrobots as an example) in 3D. This technique can in principle be integrated with microfluidic and optoelectronic chips[76] that are compatible with AC electric fields, greatly expanding the usefulness of AC levitation in colloidal sorting, assembly, and beyond.

ASSOCIATED CONTENT

Supporting Information

The Supporting Information is available free of charge at https://pubs.acs.org/doi/10.1021/acs.langmuir.3c00759.

Levitation and sedimentation of 10 μm PS microspheres when the electric field is turned on and off, respectively (MP4)

EHD flows are not sufficient or necessary for AC levitation (MP4)

https://doi.org/10.1021/acs.langmuir.3c00759
Langmuir XXXX, XXX, XXX−XXX

Controlled levitation of a few 10 μm PS microspheres to varied heights (MP4)

Controlled levitation to varied heights for 10 μm PS-Pt Janus microspheres moving via ICEP (MP4)

3D motion of a PS-Pt Janus microspheres moving via ICEP (MP4)

Dielectrophoretic attraction of 500 nm PS microspheres to the bottom electrode (MP4)

Demonstration of two levitation planes across a pair of electrodes (MP4)

Detailed descriptions of simulations, supporting experiments, and movies (PDF)

AUTHOR INFORMATION

Corresponding Author

Wei Wang − *Sauvage Laboratory for Smart Materials, School of Materials Science and Engineering, Harbin Institute of Technology (Shenzhen), Shenzhen 518055, China;* orcid.org/0000-0003-4163-3173; Email: weiwangsz@hit.edu.cn

Authors

Xiaowen Chen − *Sauvage Laboratory for Smart Materials, School of Materials Science and Engineering, Harbin Institute of Technology (Shenzhen), Shenzhen 518055, China*

Xi Chen − *Sauvage Laboratory for Smart Materials, School of Materials Science and Engineering, Harbin Institute of Technology (Shenzhen), Shenzhen 518055, China*

Yixin Peng − *Sauvage Laboratory for Smart Materials, School of Materials Science and Engineering, Harbin Institute of Technology (Shenzhen), Shenzhen 518055, China*

Lailai Zhu − *Department of Mechanical Engineering, National University of Singapore, Singapore 117575, Singapore*

Complete contact information is available at: https://pubs.acs.org/10.1021/acs.langmuir.3c00759

Notes

The authors declare no competing financial interest.

ACKNOWLEDGMENTS

The authors acknowledge helpful discussions with Prof. Jie Zhang from the University of Science and Technology of China, Prof. Shuailong Zhang from the Beijing Institute of Technology, and Prof. Carlos A. Silvera Bastia from Vanderbilt University. They thank Jiayu Liu, Xiaoxia Liu, and Prof. Xing Ma for their assistance with confocal laser scanning microscopy. They also thank the Education Center of Experiments and Innovations at HIT (Shenzhen) for their assistance with numerical simulations. X.C., X.C., Y.P., and W.W. were financially supported by the Shenzhen Science and Technology Program (RCYX20210609103122038, JCYJ20190806144807401, and JCYJ20210324121408022), and the National Natural Science Foundation of China (11774075). Lailai Zhu was supported by the Singapore Ministry of Education Tier 2 grant (MOE-T2EP50221-0012) and the A*Star AME-YIRG grant (A2084c0175).

REFERENCES

(1) Johansen, P. L.; Fenaroli, F.; Evensen, L.; Griffiths, G.; Koster, G. Optical Micromanipulation of Nanoparticles and Cells inside Living Zebrafish. *Nat. Commun.* **2016**, *7*, 10974.

(2) Alapan, Y.; Yigit, B.; Beker, O.; Demirörs, A. F.; Sitti, M. Shape-Encoded Dynamic Assembly of Mobile Micromachines. *Nat. Mater.* **2019**, *18*, 1244−1251.

(3) Sajeesh, P.; Sen, A. K. Particle Separation and Sorting in Microfluidic Devices: A Review. *Microfluid. Nanofluid.* **2014**, *17*, 1−52.

(4) Snezhko, A.; Aranson, I. S. Magnetic Manipulation of Self-Assembled Colloidal Asters. *Nat. Mater.* **2011**, *10*, 698−703.

(5) Cao, Q.; Fan, Q.; Chen, Q.; Liu, C.; Han, X.; Li, L. Recent Advances in Manipulation of Micro- and Nano-Objects with Magnetic Fields at Small Scales. *Mater. Horiz.* **2020**, *7*, 638−666.

(6) Wang, M.; He, L.; Yin, Y. Magnetic Field Guided Colloidal Assembly. *Mater. Today* **2013**, *16*, 110−116.

(7) Caleap, M.; Drinkwater, B. W. Acoustically Trapped Colloidal Crystals That Are Reconfigurable in Real Time. *Proc. Natl. Acad. Sci. U.S.A.* **2014**, *111*, 6226−6230.

(8) Dong, R.-Y.; Wang, W.; Granick, S. Colloidal Flatlands Confronted with Urge for the Third Dimension. *ACS Nano* **2019**, *13*, 9442−9448.

(9) Grier, D. G. A. A revolution in optical manipulation. *Nature* **2003**, *424*, 810−816.

(10) Mio, C.; Marr, D. W. M. Optical Trapping for the Manipulation of Colloidal Particles. *Adv. Mater.* **2000**, *12*, 917−920.

(11) Velev, O. D.; Gangwal, S.; Petsev, D. N. Particle-Localized AC and DC Manipulation and Electrokinetics. *Annu. Rep. Prog. Chem. Sect. C Phys. Chem.* **2009**, *105*, 213.

(12) Morgan, H.; Green, N. G. *AC Electrokinetics: Colloids and Nanoparticles*; Research Studies Press, 2003; Vol. *2*.

(13) Woehl, T. J.; Chen, B. J.; Heatley, K. L.; Talken, N. H.; Bukosky, S. C.; Dutcher, C. S.; Ristenpart, W. D. Bifurcation in the Steady-State Height of Colloidal Particles near an Electrode in Oscillatory Electric Fields: Evidence for a Tertiary Potential Minimum. *Phys. Rev. X* **2015**, *5*, 011023.

(14) Bukosky, S. C.; Ristenpart, W. D. Simultaneous Aggregation and Height Bifurcation of Colloidal Particles near Electrodes in Oscillatory Electric Fields. *Langmuir* **2015**, *31*, 9742−9747.

(15) Wang, K.; Leville, S.; Behdani, B.; Silvera Batista, C. A. Long-Range Transport and Directed Assembly of Charged Colloids under Aperiodic Electrodiffusiophoresis. *Soft Matter* **2022**, *18*, 5949−5959.

(16) Hashemi Amrei, S. M. H.; Bukosky, S. C.; Rader, S. P.; Ristenpart, W. D.; Miller, G. H. Oscillating Electric Fields in Liquids Create a Long-Range Steady Field. *Phys. Rev. Lett.* **2018**, *121*, 185504.

(17) Pethig, R. Review Article—Dielectrophoresis: Status of the theory, technology, and applications. *Biomicrofluidics* **2010**, *4*, 022811.

(18) Lappin, R. *Dielectrophoresis: Theory, Methodology and Biological Applications*; Wiley, 2017.

(19) Miloh, T.; Nagler, J. Travelling-Wave Dipolophoresis: Levitation and Electrorotation of Janus Nanoparticles. *Micromachines* **2021**, *12*, 114.

(20) Barnkob, R.; Rossi, M. General Defocusing Particle Tracking: Fundamentals and Uncertainty Assessment. *Exp. Fluids* **2020**, *61*, 110.

(21) Jones, T. B. *Electromechanics of Particles*; Cambridge University Press, 1995.

(22) Bukosky, S. C.; Hashemi, A.; Rader, S. P.; Mora, J.; Miller, G. H.; Ristenpart, W. D. Extreme Levitation of Colloidal Particles in Response to Oscillatory Electric Fields. *Langmuir* **2019**, *35*, 6971−6980.

(23) Ramos, A. *Electrokinetics and Electrohydrodynamics in Microsystems*; Ramos, A., Ed.; Springer Vienna: Vienna, 2011.

(24) Ishai, P. B.; Talary, M. S.; Caduff, A.; Levy, E.; Feldman, Y. Electrode Polarization in Dielectric Measurements: A Review. *Meas. Sci. Technol.* **2013**, *24*, 102001.

(25) Serghei, A.; Tress, M.; Sangoro, J. R.; Kremer, F. Electrode Polarization and Charge Transport at Solid Interfaces. *Phys. Rev. B: Condens. Matter Mater. Phys.* **2009**, *80*, 184301.

(26) Jiang, T.; Ren, Y.; Liu, W.; Tang, D.; Tao, Y.; Xue, R.; Jiang, H. Dielectrophoretic Separation with a Floating-Electrode Array Embedded in Microfabricated Fluidic Networks. *Phys. Fluids* **2018**, *30*, 112003.

(27) Ma, F.; Wu, D. T.; Wu, N. Formation of Colloidal Molecules Induced by Alternating-Current Electric Fields. *J. Am. Chem. Soc.* **2013**, *135*, 7839−7842.
(28) Markx, G. H.; Pethig, R.; Rousselet, J. The Dielectrophoretic Levitation of Latex Beads, with Reference to Field-Flow Fractionation. *J. Phys. D: Appl. Phys.* **1997**, *30*, 2470−2477.
(29) Jones, T. B.; Kraybill, J. P. Active Feedback-Controlled Dielectrophoretic Levitation. *J. Appl. Phys.* **1986**, *60*, 1247−1252.
(30) Wu, Y. C.; Koch, W. F.; Pratt, K. W. Proposed New Electrolytic Conductivity Primary Standards for KCl Solutions. *J. Res. Natl. Inst. Stand. Technol.* **1991**, *96*, 191.
(31) Bazant, M. Z.; Thornton, K.; Ajdari, A. Diffuse-Charge Dynamics in Electrochemical Systems. *Phys. Rev. E: Stat., Nonlinear, Soft Matter Phys.* **2004**, *70*, 021506.
(32) Shilov, V. N.; Delgado, A. V.; Gonzalez-Caballero, F.; Grosse, C. Thin Double Layer Theory of the Wide-Frequency Range Dielectric Dispersion of Suspensions of Non-Conducting Spherical Particles Including Surface Conductivity of the Stagnant Layer. *Colloids Surf., A* **2001**, *192*, 253−265.
(33) Yang, X.; Johnson, S.; Wu, N. The Impact of Stern-Layer Conductivity on the Electrohydrodynamic Flow Around Colloidal Motors under an Alternating Current Electric Field. *Adv. Intell. Syst.* **2019**, *1*, 1900096.
(34) Alvarez, L.; Fernandez-Rodriguez, M. A.; Alegria, A.; Arrese-Igor, S.; Zhao, K.; Kröger, M.; Isa, L. Reconfigurable Artificial Microswimmers with Internal Feedback. *Nat. Commun.* **2021**, *12*, 4762.
(35) Çetin, B.; Li, D. Dielectrophoresis in Microfluidics Technology. *Electrophoresis* **2011**, *32*, 2410−2427.
(36) Ai, Y.; Park, S.; Zhu, J.; Xuan, X.; Beskok, A.; Qian, S. DC Electrokinetic Particle Transport in an L-Shaped Microchannel. *Langmuir* **2010**, *26*, 2937−2944.
(37) Ristenpart, W. D.; Aksay, I. A.; Saville, D. A. Electrohydrodynamic Flow around a Colloidal Particle near an Electrode with an Oscillating Potential. *J. Fluid Mech.* **2007**, *575*, 83−109.
(38) An, R.; Massa, K.; Wipf, D. O.; Minerick, A. R. Solution PH Change in Non-Uniform Alternating Current Electric Fields at Frequencies above the Electrode Charging Frequency. *Biomicrofluidics* **2014**, *8*, 064126.
(39) Hashemi, A.; Miller, G. H.; Ristenpart, W. D. Asymmetric Rectified Electric Fields between Parallel Electrodes: Numerical and Scaling Analyses. *Phys. Rev. E* **2019**, *99*, 062603.
(40) Hashemi, A.; Miller, G. H.; Ristenpart, W. D. Asymmetric Rectified Electric Fields Generate Flows That Can Dominate Induced-Charge Electrokinetics. *Phys. Rev. Fluids* **2020**, *5*, 013702.
(41) Hashemi, A.; Miller, G. H.; Bishop, K. J. M.; Ristenpart, W. D. A Perturbation Solution to the Full Poisson−Nernst−Planck Equations Yields an Asymmetric Rectified Electric Field. *Soft Matter* **2020**, *16*, 7052−7062.
(42) Chen, X.; Zhou, C.; Wang, W. Colloidal Motors 101: A Beginner's Guide to Colloidal Motor Research. *Chem.—Asian J.* **2019**, *14*, 2388−2405.
(43) Wang, J. *Nanomachines: Fundamentals and Applications*; John Wiley & Sons, 2013.
(44) Pacheco, M.; López, M. Á.; Jurado-Sánchez, B.; Escarpa, A. Self-Propelled Micromachines for Analytical Sensing: A Critical Review. *Anal. Bioanal. Chem.* **2019**, *411*, 6561−6573.
(45) Parmar, J.; Vilela, D.; Villa, K.; Wang, J.; Sánchez, S. Micro- and Nanomotors as Active Environmental Microcleaners and Sensors. *J. Am. Chem. Soc.* **2018**, *140*, 9317−9331.
(46) Marchetti, M. C.; Joanny, J. F.; Ramaswamy, S.; Liverpool, T. B.; Prost, J.; Rao, M.; Simha, R. A. Hydrodynamics of Soft Active Matter. *Rev. Mod. Phys.* **2013**, *85*, 1143−1189.
(47) Needleman, D.; Dogic, Z. Active Matter at the Interface between Materials Science and Cell Biology. *Nat. Rev. Mater.* **2017**, *2*, 17048.
(48) Xiao, Z.; Wei, M.; Wang, W. A Review of Micromotors in Confinements: Pores, Channels, Grooves, Steps, Interfaces, Chains, and Swimming in the Bulk. *ACS Appl. Mater. Interfaces* **2019**, *11*, 6667−6684.
(49) Wei, M.; Zhou, C.; Tang, J.; Wang, W. Catalytic Micromotors Moving Near Polyelectrolyte-Modified Substrates: The Roles of Surface Charges, Morphology, and Released Ions. *ACS Appl. Mater. Interfaces* **2018**, *10*, 2249−2252.
(50) Chiang, T.-Y.; Velegol, D. Localized Electroosmosis (LEO) Induced by Spherical Colloidal Motors. *Langmuir* **2014**, *30*, 2600−2607.
(51) Ketzetzi, S.; de Graaf, J.; Doherty, R. P.; Kraft, D. J. Slip Length Dependent Propulsion Speed of Catalytic Colloidal Swimmers near Walls. *Phys. Rev. Lett.* **2020**, *124*, 048002.
(52) Ketzetzi, S.; de Graaf, J.; Kraft, D. J. Diffusion-Based Height Analysis Reveals Robust Microswimmer-Wall Separation. *Phys. Rev. Lett.* **2020**, *125*, 238001.
(53) Yang, T.; Tomaka, A.; Tasci, T. O.; Neeves, K. B.; Wu, N.; Marr, D. W. M. Microwheels on Microroads: Enhanced Translation on Topographic Surfaces. *Sci. Robot.* **2019**, *4*, 4.
(54) Jalilvand, Z.; Pawar, A. B.; Kretzschmar, I. Experimental Study of the Motion of Patchy Particle Swimmers Near a Wall. *Langmuir* **2018**, *34*, 15593−15599.
(55) Boymelgreen, A.; Yossifon, G. Observing Electrokinetic Janus Particle−Channel Wall Interaction Using Microparticle Image Velocimetry. *Langmuir* **2015**, *31*, 8243−8250.
(56) Bianchi, S.; Saglimbeni, F.; Di Leonardo, R. Holographic Imaging Reveals the Mechanism of Wall Entrapment in Swimming Bacteria. *Phys. Rev. X* **2017**, *7*, 011010.
(57) Xiao, Z.; Duan, S.; Xu, P.; Cui, J.; Zhang, H.; Wang, W. Synergistic Speed Enhancement of an Electric-Photochemical Hybrid Micromotor by Tilt Rectification. *ACS Nano* **2020**, *14*, 8658−8667.
(58) Uspal, W. E.; Popescu, M. N.; Dietrich, S.; Tasinkevych, M. Guiding Catalytically Active Particles with Chemically Patterned Surfaces. *Phys. Rev. Lett.* **2016**, *117*, 048002.
(59) Uspal, W. E.; Popescu, M. N.; Dietrich, S.; Tasinkevych, M. Self-Propulsion of a Catalytically Active Particle near a Planar Wall: From Reflection to Sliding and Hovering. *Soft Matter* **2015**, *11*, 434−438.
(60) Zhou, C.; Suematsu, N. J.; Peng, Y.; Wang, Q.; Chen, X.; Gao, Y.; Wang, W. Coordinating an Ensemble of Chemical Micromotors via Spontaneous Synchronization. *ACS Nano* **2020**, *14*, 5360−5370.
(61) Das, S.; Garg, A.; Campbell, A. I.; Howse, J.; Sen, A.; Velegol, D.; Golestanian, R.; Ebbens, S. J. Boundaries Can Steer Active Janus Spheres. *Nat. Commun.* **2015**, *6*, 8999.
(62) Simmchen, J.; Katuri, J.; Uspal, W. E.; Popescu, M. N.; Tasinkevych, M.; Sánchez, S. Topographical Pathways Guide Chemical Microswimmers. *Nat. Commun.* **2016**, *7*, 10598.
(63) Campbell, A. I.; Ebbens, S. J. Gravitaxis in Spherical Janus Swimming Devices. *Langmuir* **2013**, *29*, 14066−14073.
(64) Zhou, C.; Zhang, H. P.; Tang, J.; Wang, W. Photochemically Powered AgCl Janus Micromotors as a Model System to Understand Ionic Self-Diffusiophoresis. *Langmuir* **2018**, *34*, 3289−3295.
(65) Singh, D. P.; Uspal, W. E.; Popescu, M. N.; Wilson, L. G.; Fischer, P. Photogravitactic Microswimmers. *Adv. Funct. Mater.* **2018**, *28*, 1706660.
(66) Ren, L.; Nama, N.; McNeill, J. M.; Soto, F.; Yan, Z.; Liu, W.; Wang, W.; Wang, J.; Mallouk, T. E. 3D Steerable, Acoustically Powered Microswimmers for Single-Particle Manipulation. *Sci. Adv.* **2019**, *5*, No. eaax3084.
(67) Ren, L.; Wang, W.; Mallouk, T. E. Two Forces Are Better than One: Combining Chemical and Acoustic Propulsion for Enhanced Micromotor Functionality. *Acc. Chem. Res.* **2018**, *51*, 1948−1956.
(68) Gangwal, S.; Cayre, O. J.; Bazant, M. Z.; Velev, O. D. Induced-Charge Electrophoresis of Metallodielectric Particles. *Phys. Rev. Lett.* **2008**, *100*, 058302.
(69) MBoymelgreen, A.; Kunti, G.; Garcia-Sanchez, P.; Ramos, A.; Yossifon, G.; Miloh, T.; Miloh, T. The Role of Particle-Electrode Wall Interactions in Mobility of Active Janus Particles Driven by Electric Fields. *J. Colloid Interface Sci.* **2022**, *616*, 465−475.

https://doi.org/10.1021/acs.langmuir.3c00759
Langmuir XXXX, XXX, XXX−XXX

(70) Chen, X.; Chen, X.; Elsayed, M.; Edwards, H.; Liu, J.; Peng, Y.; Zhang, H. P.; Zhang, S.; Wang, W.; Wheeler, A. R. Steering Micromotors via Reprogrammable Optoelectronic Paths. *ACS Nano* **2023**, *17*, 5894−5904.
(71) Piazza, R. Settled and Unsettled Issues in Particle Settling. *Rep. Prog. Phys.* **2014**, *77*, 056602.
(72) Evander, M.; Nilsson, J. Acoustofluidics 20: Applications in Acoustic Trapping. *Lab Chip* **2012**, *12*, 4667.
(73) Boymelgreen, A. M.; Balli, T.; Miloh, T.; Yossifon, G. Active Colloids as Mobile Microelectrodes for Unified Label-Free Selective Cargo Transport. *Nat. Commun.* **2018**, *9*, 760.
(74) Guo, J.; Gallegos, J. J.; Tom, A. R.; Fan, D. Electric-Field-Guided Precision Manipulation of Catalytic Nanomotors for Cargo Delivery and Powering Nanoelectromechanical Devices. *ACS Nano* **2018**, *12*, 1179−1187.
(75) Gangwal, S.; Cayre, O. J.; Velev, O. D. Dielectrophoretic Assembly of Metallodielectric Janus Particles in AC Electric Fields. *Langmuir* **2008**, *24*, 13312−13320.
(76) Zhang, S.; Xu, B.; Elsayed, M.; Nan, F.; Liang, W.; Valley, J. K.; Liu, L.; Huang, Q.; Wu, M. C.; Wheeler, A. R. Optoelectronic Tweezers: A Versatile Toolbox for Nano-/Micro-Manipulation. *Chem. Soc. Rev.* **2022**, *51*, 9203−9242.

https://doi.org/10.1021/acs.langmuir.3c00759
Langmuir XXXX, XXX, XXX−XXX